ACS MATERIALS Au
AN OPEN ACCESS JOURNAL OF THE AMERICAN CHEMICAL SOCIETY

pubs.acs.org/materialsau
Article

Bioinspired Composite Materials with Amplified Clusteroluminescence: Chemodosimetric Interaction Targeting Hypochlorite in Aqueous Medium

Published as part of ACS Materials Au special issue "2024 Rising Stars".

Rikitha S Fernandes and Nilanjan Dey*

Cite This: *ACS Mater. Au* 2025, 5, 308−319
Read Online

ACCESS | Metrics & More | Article Recommendations | Supporting Information

ABSTRACT: Owing to the advantages of cellulose such as exceptional biocompatibility and biodegradability, we synthesized cellulose-grafted bisindolyl methane (BIM) (**1. Cell**) composite. This biobased smart material was used as an effective colorimetric and fluorescent sensor for hypochlorite in the aqueous medium with a detection limit of 0.02 μM. Interestingly, cellulose exhibited inherent clusteroluminescence in solution, which was further intensified by the probe acting as a dopant. Both the boronic acid and bisindole groups in probe **1** are essential for this enhanced fluorescence, as boronic acid enables boronate ester formation with cellulose, while the bisindole groups facilitate additional hydrogen bonding interactions. This unique dual functionality produces a strong, solution-phase clusteroluminescent effect, creating a rigid microenvironment that promotes long-range exciton migration and an amplified fluorescence response. Furthermore, the **1. Cell** exhibited ∼2.8-fold quenching, while probe **1** alone exhibited negligible fluorescence change in the presence of hypochlorite. Mechanistic investigation reveals that the probe formed a boronate ester via the interaction with cellulose, which was subsequently cleaved in the presence of hypochlorite. The differences in the response might be attributed to the distinct nature of their self-assemblies; **1. Cell** could form long-range highly ordered aggregates, while probe **1** alone in the aqueous medium resulted in spontaneous random aggregates. Additionally, we employed cellulose paper strips to explore the practicability of the probe as a paper-based sensor. The chemically modified paper strips, grafted with probe molecules, were found to be stable for a week and could effectively detect hypochlorite in the presence of interfering analytes via the naked eye and fluorescent color-changing response.

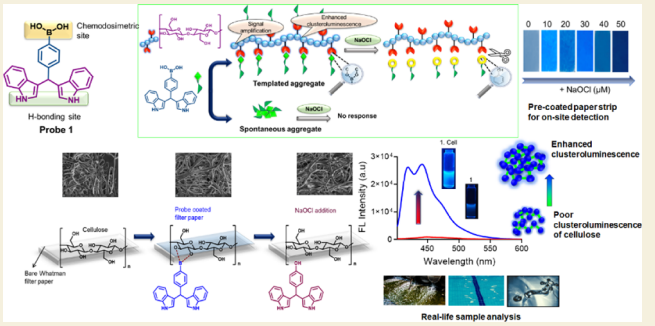

KEYWORDS: *templated aggregate, hypochlorite, paper-based device, boronate ester, BIM, loose-bolt effect, clusteroluminescence*

INTRODUCTION

Clusteroluminescence (CL), typically a property observed in solid-state or highly aggregated systems, arises from tightly packed clusters that limit molecular motion and enhance radiative decay. Upon excitation from the ground state (S_0) to the excited state (S_1), some excitons release energy via a through-space conjugation (TSC) radiative pathway, emitting short-wavelength light. Others relax to a lower-energy state through TSC, producing long-wavelength CL. The CL efficiency depends on the strength of TSC interactions and the stability of the conformation, which is influenced by a rigid molecular structure and intermolecular interactions.[1] Clusteroluminogens show promise for encryption and bioimaging but require significantly higher concentrations for imaging, limiting practical use. Additionally, poor analyte interaction in solution reduces their sensing effectiveness. Therefore, new strategies to enhance the clustering-triggered emission (CTE) effect are crucial for achieving strong luminescence at lower concentrations in solution.[2,3]

Unlike conventional aggregation-induced emission (AIE) materials, CTE luminogens are inherently hydrophilic, easy to synthesize, and exhibit high biocompatibility, providing significant advantages for functional materials in biotechnological applications.[1,4] Unlike other polymers, cellulose and its nanoderivatives exhibit clusteroluminescence due to their unique molecular structure, characterized by dense hydrogen bonding and organized aggregation. This tightly packed,

Received: September 7, 2024
Revised: November 28, 2024
Accepted: December 2, 2024
Published: December 13, 2024

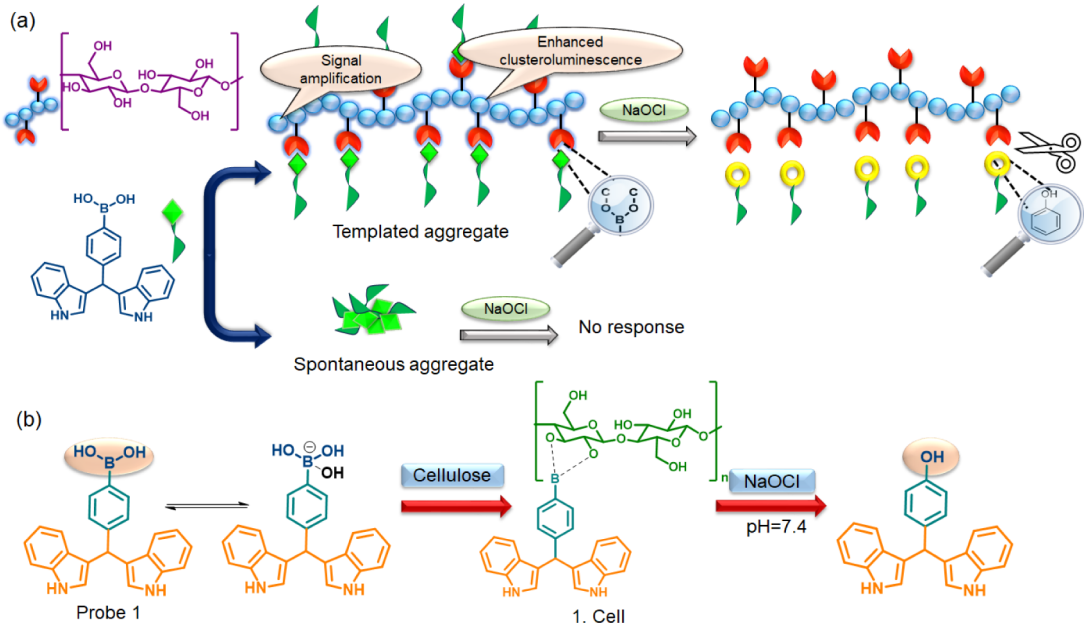

Figure 1. (a) Schematic representation of the mechanism of hypochlorite-mediated response of the **1. Cell** and probe **1**. (b) Dynamic covalent nature of the probe in the presence of cellulose, followed by the mechanistic pathway of hypochlorite detection.

hydrogen-bonded network restricts nonradiative pathways, stabilizes exciton formation and enhances emission, allowing faint blue emissions in solid states without aromatic or conjugated systems. As a natural, nontoxic, and biocompatible polymer, it is highly valued as a functional material due to its structural strength, durability, and flexibility, making it suitable for flexible wearables and electronics.[1,4]

On the other hand, many ICT-based boronic acid fluorophores have been developed as hypochlorite sensors, which mostly exploit its potent oxidizing ability.[5] However, these probes face challenges, including low water solubility, background fluorescence, interference from other reactive oxygen species (ROS), complex synthesis, and a limited pH range. Therefore, there is an ongoing demand for fluorescent chemosensors with better water solubility, sensitivity, and selectivity for hypochlorite. Supramolecular and dynamic polymers, known for their reversible and degradable properties, offer promising avenues in polymer science for the creation of innovative sensing materials. Dynamic covalent chemistry has become a key strategy for designing such functional polymer networks, merging the robustness of chemically cross-linked systems with the adaptability of physical cross-links.[6] In dynamic covalent chemistry, reaction pathways are governed by thermodynamic control, resulting in products that are both reversible and robust, maintained by strong covalent bonds.[7] In this regard, boronic acid derivatives, upon reversible interaction with diols, have led to the formation of cyclic boronate esters and are useful to construct reversible molecular assemblies and a wide range of hierarchical structures.[8] The dynamic nature of boronates often results in predictable geometries of large molecular aggregates and assemblies. This capability allows researchers to finely tune the structural, electronic, catalytic, sensing, and other chemical properties of these compounds. Most studies in this area have focused on aqueous systems, particularly exploring reactions between boronic acids and aliphatic 1,2- or 1,3-dihydroxy motifs in saccharides and glycosylated biomolecules.[9]

Inspired by both the CTE phenomenon and dynamic covalent chemistry, we propose a novel approach to enhance the CTE effect of cellulose in dilute solutions (Figure 1). We developed a biobased smart composite (**1. Cell**) by functionalizing cellulose with easily synthesizable BIM-based boronic acid probe (probe **1**) for the detection of hypochlorite in the aqueous medium (pH 7.4). The probe incorporates a bisindolyl functionality and a boronic acid functionality, which forms hydrogen bonds and boronate ester (via chemodosimetric interaction) with the cellulose, respectively, and further promotes the inherent clusteroluminescence of cellulose. The **1. Cell** composite displayed a significant fluorescence quenching (~2.8-fold) in the presence of hypochlorite, accompanied by a fluorescent color change from bright blue to faint blue. Mechanistic investigation confirms that the hypochlorite-induced fluorescence changes of the **1. Cell** composite was due to the cleavage of the boronate ester moiety to the phenolic −OH moiety, resulting from the oxidative transformation of the electron-withdrawing C−B bond to the electron donating C−O bond. Unlike the synthetic probes, the cellulose-based sensor, , is biodegradable and biocompatible, aligning with green chemistry principles and providing a sustainable alternative.[10] Our system leverages the enhanced clusteroluminescence of cellulose by using the probe as an organic dopant within the cellulose matrix. This dopant effect increases the inherent clusteroluminescence of cellulose through a structured aggregation of BIM chromophores, promoting exciton migration and signal amplification. As a result, the sensor exhibits enhanced fluorescence sensitivity and selectivity via cluster luminescence, which is rarely achievable in solution-based systems. Finally, unlike many traditional sensors that lack stability in practical applications,[10] our cellulose-based paper strips offer stable, portable detection with visible color and fluorescence changes and remain effective for up to a week, thus supporting on-site testing of hypochlorite. This article presents the potential of BIM-cellulose complexation as a novel approach to modulate

https://doi.org/10.1021/acsmaterialsau.4c00113
ACS Mater. Au 2025, 5, 308−319

the clusteroluminescent properties in these systems and further be employed for hypochlorite detection.

EXPERIMENTAL SECTION

All chemicals were procured from reputable chemical vendors. FTIR spectra (in wavenumbers (cm^{-1})) were recorded on a PerkinElmer FT-IR Spectrum BX system. Meanwhile, ^{1}H and ^{13}C NMR spectra were obtained with a Bruker Avance Neo 400 spectrometer operating at 400 and 100 MHz for ^{1}H and ^{13}C NMR spectroscopy, respectively. Mass spectra were recorded using Shimadzu LC-MS.

Spectroscopic Studies

The UV−vis spectroscopic studies were conducted on a JASCO (model V-650) UV−vis spectrophotometer with a slit-width of 5 nm. Sensing was performed by adding requisite amounts of sodium hypochlorite to aqueous solutions of probe **1** (10×10^{-6} M). Fluorescence experiments were carried out using FluoroLog-TM (Horiba Scientific), maintaining a slit-width of 5 nm for both excitation and emission. The excitation wavelength was set at 390 nm.

Fluorescence Decay Experiment

Fluorescence lifetime values were recorded using a time-correlated single photon counting fluorimeter (Horiba Jobin Yvon). Average fluorescence lifetimes (τ_{av}) were calculated from

$$\tau_{av} = (a_1\tau_1^2 + a_2\tau_2^2 + a_3\tau_3^2)/(a_1\tau_1 + a_2\tau_2 + a_3\tau_3)$$

where a_1, a_2 and a_3 are the relative amplitudes and τ_1, τ_2, and τ_3 are the lifetime values, respectively. Data fitting was performed by using EZ Time software.

Dynamic Light Scattering Studies (DLS)

DLS measurements were conducted using a Malvern Zetasizer NanoZS particle sizer (Malvern Instruments Inc., MA) instrument. Two mL of probe stock solutions (1 mM) was prepared in DMSO and diluted with water to the final concentration of 10 μM with/without cellulose. Before recording, the samples were mixed thoroughly to obtain a uniform suspension in water.

Scanning Electron Microscopy (SEM)

Samples for SEM were drop casted on a silicon wafer with the required concentrations, and the solvent was allowed to evaporate overnight. The silicon wafer was then sputter-coated using a Leica Ultra Microtome EM UC7, and the stubs were loaded into an FEI Apreo LoVac to obtain images at 1 μm magnification

Small/Wide Angle X-ray Scattering (SAXS/WAXS)

The Nano-inXider SW-L SAXS/WAXS System with dual detector (Xenocs SAS, France) was used for WAXS measurements for the probe **1**, cellulose and probe **1**. Cellulose. The data obtained were analyzed using Xenocs XSACT Software.

X-ray Photoelectron Spectroscopy (XPS)

Thermo Fisher Scientific K-Alpha instrument (Thermo Fisher Scientific Pvt. Ltd., UK) was utilized to conduct XPS measurements for probe **1**, cellulose, and probe **1**. Cellulose.

RESULTS AND DISCUSSION

Design and Synthesis of Probe Molecule

The probe **1** was synthesized according to the procedure reported in literature (Scheme. S1),[11] and was characterized by ^{1}H NMR, ^{13}C NMR, and LC-MS.[12] Bis(indolyl)methane derivatives (BIMs) have been employed as valuable hydrogen bond donors in sensor applications. Notably, the color and optical properties of BIMs are markedly influenced by the extent of π conjugation within the system, electronic properties of the aryl moiety positioned at the meso site, and the inherent conformational flexibility. On the other hand, boronic acid serves as an active intermediate with notable water solubility and photostability. This Lewis acid−base interaction prompts the boron atom to undergo interconversion between an uncharged trigonal planar structure and an anionic tetravalent borate species.[13] The probe **1** features two distinct receptor sites, namely, the boronic acid (for boronate ester formation) and indole (via -NH interaction), that can bind with cellulose chains via covalent and noncovalent interactions, respectively. The dual binding capability of probe **1** creates a robust, multifunctional interaction framework ideal for high-performance, biocompatible sensor systems, thereby enhancing its selectivity and responsiveness in sensing applications.

Investigation of Photophysical Properties

In the aqueous medium (pH 7.4), the UV−visible spectrum of probe **1** displayed an absorption band at the 495 nm region, attributed to the intramolecular charge transfer (ICT) from indole substituent to the phenylboronic acid functionality. Additionally, a prominent tailing was observed on the lower-energy region of the absorption spectrum, which is quite expected for colloidal chromophoric aggregates due to Mie scattering in the aqueous solution (Figure 2a).[14−16] In

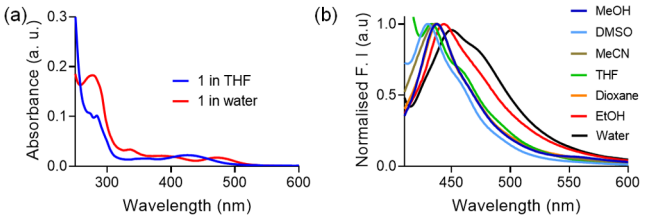

Figure 2. (a) UV−visible spectra of **1** (10 μM) in THF and water. (b) Fluorescence spectra of **1** (10 μM, λ_{ex} = 390 nm) in different solvents.

addition, the absorbance at ∼280 nm is attributable to the electronic transitions associated with the indole units. Furthermore, the solvatochromic behavior of probe **1** was investigated in a broad range of solvents such as hexane, tetrahydrofuran, dioxane, acetonitrile, dimethylformamide, dimethyl sulfoxide, ethanol, and methanol (Figure 2b). We observed the broadening of the fluorescence spectrum in polar solvents along with a red shift (∼33 nm) of emission maximum from 430 to 463 nm upon moving from THF to water. Additionally, there was a significant diminution in the fluorescence intensity of the probe in the water medium, attributed to the increasing solvent polarity, which stabilizes the excited state of the probe and reduces its emission energy.

The fluorescence spectrum of **1** (λ_{ex} = 390 nm) displayed vibronic bands, along with a small hump at 434 nm in THF medium. Nevertheless, we observed a broad fluorescence spectrum with emission maxima centered at 460 nm in aqueous medium. To know whether this broad spectrum in the aqueous medium is due to emission by single or multiple photoactive species, we recorded the excitation spectra of **1** over the emission wavelength range from 425 to 490 nm. We observed that the excitation spectra corresponding to the longer wavelength region exhibited very distinct features compared to the spectra obtained at the shorter wavelength region (Figure S1). For instance, the excitation spectrum corresponding to the 460 nm emission band showed a major peak at 285 nm, whereas the excitation spectrum assigned to the 494 nm band showed an additional peak at the ∼375 nm region, which suggests the presence of at least two photoactive species in equilibrium. Nevertheless, we performed DLS

https://doi.org/10.1021/acsmaterialsau.4c00113
ACS Mater. Au 2025, 5, 308−319

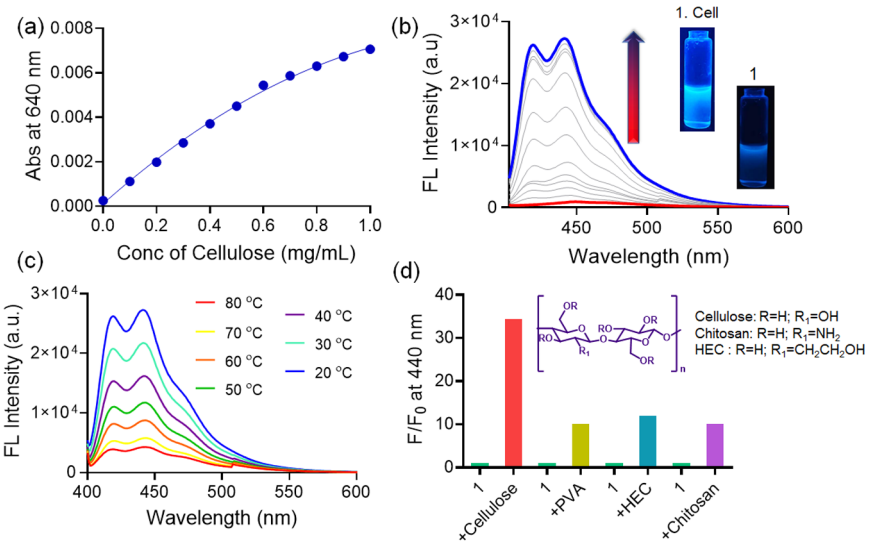

Figure 3. (a) UV−visible spectra of probe **1** (10 μM) upon cellulose addition (0−1 mg/mL) in water. (b) Fluorescence spectra of **1** (10 μM, λ_{ex} = 390 nm) upon cellulose addition (0−1 mg/mL) in water. (c) Temperature-dependent fluorescence spectra of probe **1. Cell** (10 μM, λ_{ex} = 390 nm) in water. (d) Change in fluorescence intensity of probe **1** at 440 nm upon addition of various biopolymers (10 equiv) in water.

studies of **1** in aqueous medium (PBS buffer, pH 7.4) and the hydrodynamic diameter was found to be 156.4 ± 11 nm. This indicated the formation of nanoscopic self-assemblies, which was further evident by the FESEM images (Figure S2). Additionally, fluorescence lifetime experiments (TCSPC) were conducted for probe **1** to understand the decay kinetics of the excited-state photoactive species. The compound exhibited a biexponential decay profile in THF with an average lifetime of ∼5.02 ns, while a multiexponential decay with an average lifetime of ∼3.72 ns was observed in the aqueous medium. The multiexponential decay curves in water are interpreted as a convolution of multiple continuous components, reflecting the presence of diverse molecular environments within the amphiphilic aggregated structures.[17]

It was observed that the probe exhibited a low inherent fluorescence and hence low quantum yield in aqueous medium. The O−H bond vibrations in water can quench the fluorescence of the probe by converting electronic excitation energy to vibrational energy. Similarly, intramolecular alcohols or carboxylic acids can absorb this energy through internal conversion, thereby reducing the fluorescence quantum yield. This is known as the "loose-bolt effect" where, like a loose bolt absorbing energy from a motor's vibrations, a high-frequency rotor in resonance with an excited state absorbs energy. Thus, the loose-bolt effect enhances internal conversion by dissipating electronic energy through vibrations of -$B(OH)_3^-$ in aqueous medium.[18,19]

Design and Characterization of Composite Materials

Lately, researchers have surface-modified cellulose to improve hydrophobicity, adhesion, and solubility for applications in bioimaging and diagnostics.[20] The large surface area and abundant hydroxyl groups of cellulose enable easy modification, making it ideal for incorporating fluorescent probes for bioimaging, and diagnostics. However, strong hydrogen bonding and high crystallinity still pose challenges in synthesizing fluorescent cellulose derivatives with good solubility.[21] On the other hand, in aqueous environments, the free diol (here, cellulose) and the diol bound in the boronate ester exist in dynamic equilibrium, with a kinetically controlled dynamic exchange between the reactants (free diol and boronic acid) and the products (boronate ester) through a low-energy transition state. The ease of exchange between the bound and free species classifies boronate and boronic esters as "dynamic covalent" structures.[22]

Thus, herein we have prepared a composite of the probe with cellulose in a pH 7.4 medium. Upon incremental addition of cellulose to the aqueous solution of the probe, we observed a broadening of absorption spectra along with prominent tailing extending into the longer wavelength region (Figure 3a). This could be attributed to the aggregate formation due to Mie scattering, as expected for colloidal chromophoric aggregates.[23] In addition, the observed aggregation could also be due to the result of reduced electrostatic repulsions relative to van der Waals attractions.[24] Additionally, a change in the surface charge of cellulose upon incorporation of the probe would have influenced aggregation.[25]

Furthermore, upon excitation at 390 nm, probe **1** exhibits ∼29.3-fold fluorescence enhancement along with a concomitant blue shift (∼8 nm) with maxima centered at 440 and 418 nm in the presence of cellulose (Figure 3b). The fluorescence enhancement is primarily due to the increased clusteroluminescence of cellulose facilitated by boronate ester linkages. These linkages rigidify the cellulose matrix, restricting molecular flexibility and amplifying the luminescent efficiency. Higher densities of cross-links further reinforce the network, promoting intermolecular and intramolecular clusterization and thereby yielding sharp emission bands. Additionally, extensive hydrogen bonding in the cellulose matrix contributes to conformational rigidification, enhancing fluorescence.[3,4] Notably, the probe itself exhibits negligible fluorescence in the aqueous medium, confirming that the observed fluorescence enhancement originates exclusively from the increased clusteroluminescence of the cellulose matrix. Furthermore, the solvent-dependent fluorescence behavior of the probe suggests that the fluorescence enhancement in the presence of cellulose cannot be attributed to a shift in the solvent polarity but rather to the enhanced clusteroluminescence of cellulose upon probe binding. Therefore, the templated aggregate of **1. Cell** rely on synergistic noncovalent

https://doi.org/10.1021/acsmaterialsau.4c00113
ACS Mater. Au 2025, 5, 308−319

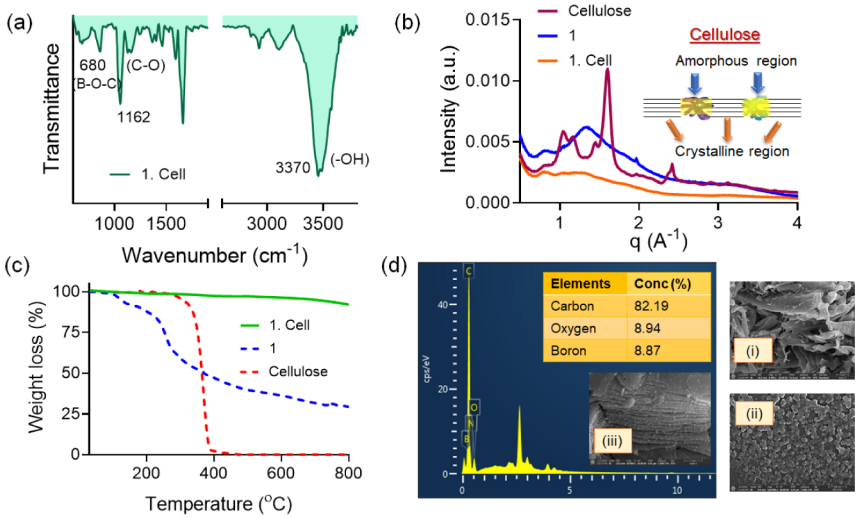

Figure 4. (a) FTIR spectra of **1. Cell**. (b) WAXS pattern of probe **1**, cellulose and **1. Cell**. (c) TGA profile of **1**, cellulose and **1. Cell**. (d) EDAX of **1. Cell** and FESEM images of (i) Cellulose (ii) probe **1** and (iii) **1. Cell**.

interactions, such as electrostatic interaction, hydrogen bond, coordination interaction, hydrophobic interaction, van der Waals force, and so on.

To confirm the role of boronic acid moiety in enhancing the clusteroluminescence of cellulose, we conducted fluorescence experiments with probe **3** (benzene ring in the meso position of BIM) in the presence of cellulose (Figure S3a and b). While the incorporation of probe **3** led to some enhancement in cellulose fluorescence, the extent of enhancement was significantly lower compared to that of probe **1**. This highlights the critical role of the boronic acid functionality in the fluorescence enhancement of cellulose. This functionality facilitates boronate ester formation, which rigidifies the cellulose matrix, suppressing nonradiative decay pathways and thereby enhancing clusteroluminescence.

Furthermore, to confirm the importance of incorporating the indole moiety, we conducted fluorescence experiments with phenylboronic acid (probe **2**). Upon introduction of cellulose into the solution of probe **2**, we observed an increase in fluorescence intensity. However, the degree of fluorescence enhancement observed with probe **2** was less pronounced compared to that with probe **1**. This suggests that while the boronic acid functionality is crucial for inducing clusteroluminescence, the indole groups play a pivotal role in amplifying the luminescent response. The bisindole functionality likely participates in additional interactions, such as hydrogen bonding between the −NH groups of indoles and the hydroxyl groups of cellulose. The incorporation of such polycyclic aromatic hydrophobic moieties fosters stronger noncovalent interactions, with the cellulose matrix, facilitating better alignment and rigidification of the framework.

These results indicate that neither the boronic acid nor the bisindole groups alone is sufficient to maximize fluorescence enhancement. Instead, the combination of both functionalities in probe **1** i.e., boronic acid groups for boronate ester formation and bisindole groups for potential hydrogen bonding creates an optimal interaction with cellulose, resulting in a marked increase in clusteroluminescence. This unique dual functionality enables probe **1** to effectively enhance the inherent clusteroluminescence of cellulose, underscoring the critical role of both boronic acid and bisindole groups in achieving a strong, solution-phase fluorescence enhancement.

Compared to the free probe **1** (τ= 3.72 ns), the **1. Cell** was found to show a longer fluorescence average lifetime (τ= 5.68 ns). The prolonged lifetime infers a slower decay, due to the mobility-restricted region whereas the shorter lifetime of the free probe is a result of nonradiative pathways present for fluorophores owing to an increase in mobility in solution.[26] This promotes energy loss to the surrounding medium via nonradiative processes.[27] In addition, the formation of boronate ester has been reported to show a longer fluorescence lifetime.[28,29] Additionally, we investigated the temperature-dependent fluorescence response of the **1. Cell** in aqueous medium (Figure 3c). Upon increasing the solution temperature from 20 to 80 °C, the fluorescence intensity decreased, plausibly due to the disruption/dissociation of the **1. Cell** templated aggregate.[23] At elevated temperatures, the noncovalent interactions, particularly hydrogen bonding, between probe molecules and cellulose weaken, leading to the dissociation of the structured aggregates, thereby reducing clusteroluminescence. The disruption of this ordered assembly diminishes the spatial confinement and local rigidity required to sustain efficient clusteroluminescent emission. Consequently, the fluorescence intensity decreases with increasing temperature as the molecular environment becomes less favorable for sustaining efficient clusteroluminescent emission. Nevertheless, we also checked if other biopolymers such as Chitosan and synthetic polymers such as PVA (Poly (vinyl alcohol)), HEC (hydroxy ethyl cellulose) could induce a similar fluorescence response as that of cellulose upon binding to the probe (Figure 3d). We observed that these biopolymers exhibited a turn-on fluorescent response with the probe, but the extent of interaction was quite less as compared to the cellulose. The selective fluorescence response with cellulose, unlike that with chitosan, PVA, and HEC, is due to dense hydroxyl groups and the inherent clusteroluminescence of cellulose. These hydroxyl groups form strong boronate ester linkages with probe **1**, enhancing the inherent fluorescence of cellulose by leveraging its compact hydrogen-bonded network. Additionally, only cellulose allows probe **1** to utilize both of its binding sites: the boronic acid site for ester formation and the indole site for interaction via −NH bonding. This dual binding is unique to cellulose and significantly contributes to its enhanced fluorescence response. The flexible torsion angles in

https://doi.org/10.1021/acsmaterialsau.4c00113
ACS Mater. Au 2025, 5, 308−319

chitosan, PVA, and HEC result in weaker fluorescence and lack clusteroluminescent enhancement. In contrast, the fixed torsion angles of cellulose provide a rigid, ordered structure that promotes stronger interactions and fluorescence enhancement upon binding with probe **1**.[30]

The FTIR analysis of the composite reveals the broad band around 3370 cm^{-1} due to the O−H stretching.[31] The characteristic bands at 1437 and 680 cm^{-1} are ascribed to the B−O and B−O−C stretching vibrations respectively (Figure 4a). In addition, the broad IR range from 1355 to 1422 cm^{-1} was attributed to the B−C stretching of the boronate ester. The IR bands at 1162 and 1241 cm^{-1} correspond to C−O stretching of the boronate ester ring.[32,33] Furthermore, the FTIR spectrum of the probe exhibits peaks at 1310 and 1086 cm^{-1}, which are attributed to B−O stretching and C−B stretching and disappear in the FTIR spectra of the composite.[33,34] The broad IR band (3266−3666 cm^{-1}) suggests the presence of hydrogen bonding interactions, likely involving the NH group of the indole moiety with the hydroxyl groups of cellulose.

Furthermore, WAXS analysis revealed that the incorporation of the probe into the cellulose matrix decreased the crystallinity of the formed composite (Figure 4b). The WAXS pattern of pristine cellulose shows that the diffraction pattern exhibiting peaks at 1.56, and 2.44 was ascribed to the crystalline regions of cellulose, and was superimposed by a broad amorphous halo at 1.03.[35] The highest peak (q = 1.56) of pristine cellulose corresponds to the [002] crystallographic planes, whose intensity gives information regarding the extent of crystallinity. On the other hand, the peaks of the **1. Cell** composite was quite broad (q = 1.3), with lower peak intensities, signifying that the original crystalline structures of the cellulose were destroyed upon binding with the probe. Additionally, the broadening might also be attributable to the finite sizes of the cellulose crystallites and imperfections in the crystals upon composite formation.[36] These findings suggest that the diffraction peaks significantly reduced upon grafting, and the composite comprised a less ordered cellulose crystalline structure than that of the pristine cellulose. These findings unequivocally confirm the successful integration of the recognition sites of the probe into the cellulose structure.

Cellulose, a linear polymer of glucose units, forms crystalline regions easily, and hence, its thermal stability can be altered via chemical modification. The **1. Cell** composite was found to show superior thermal stability when compared to the probe and pristine cellulose, as evidenced by the TGA profiles (Figure 4c). Before 380 °C, the weight loss of the composite and cellulose is similar, but at higher temperatures, the thermal stability of the composite is quite higher than pristine cellulose. This increased thermal stability was possibly due to the altered chemical structure and crystallinity of cellulose in **1. Cell**. Furthermore, the FESEM images of the composite reveal that the surface was observed to be rough, multilayered, and almost lost the original spherical structures and fiber-like structure of the probe and cellulose, respectively (Figure 4d). This could probably be due to the damage of the microstructure of cellulose upon grafting the probe onto it. Additionally, the EDAX of **1. Cell** confirms the increase in the amount of carbon, oxygen, and boron upon interaction with cellulose (Figure 4d). Upon comparison of elemental analysis of the **1** with the **1. Cell**, it was found that the carbon content of the composite increased from 39.54 to 82.19%, and the oxygen content of the composite also increased (from 8.02 to 8.94%) and boron content from 8.24 to 8.87%.

Furthermore, XPS analysis was employed to comprehensively characterize the surface composition and electronic states of the constituent elements in the composite. The XPS survey spectra of the composite specify the presence of the B, N, O, and C elements. In the B 1s spectrum of probe **1**, the peaks at 187.78 eV and 190.1 represented the B−C and B−O bonds,[37] which increased to 190.96 and 192.85 eV upon composite formation (Figure 5a). In O 1s core-level spectrum

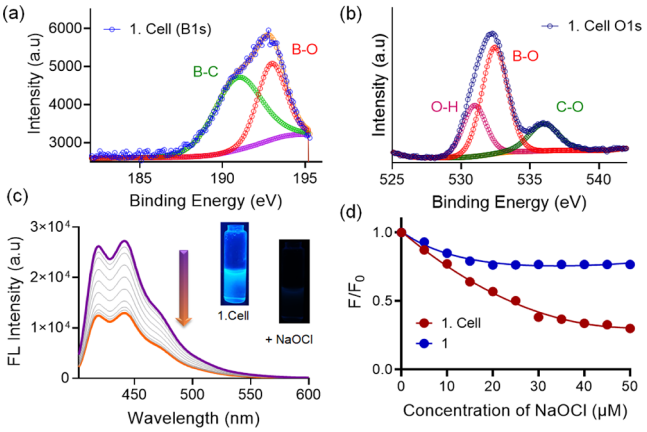

Figure 5. (a) XPS spectra of B 1s of **1. Cell** composite. (b) XPS spectra of O 1s of **1. Cell** composite. (c) Fluorescence spectra of **1. Cell** (10 μM, λ_{ex} = 390 nm) upon addition of hypochlorite (0−50 μM) in water. (d) Change in fluorescence intensity of probe **1** and **1. Cell** (at 440 nm) in the presence of hypochlorite (0−50 μM) in water.

of the probe (Figure 5b), the peaks at 530.6, 532.3, and 534.22 eV are ascribed to O−H, O−B, and C−O bonds respectively, which further changed to 529.92, 533.5, and 536 eV in the composite.[38,39] These results confirmed that the probe and cellulose were cross-linked by the boron ester bond, which was consistent with the elemental analysis.

Optical Response to Hypochlorite

As a constant effort in designing probes for the detection of biologically relevant analytes, we investigated the sensing behavior of the composite toward hypochlorite in a pure aqueous medium (pH 7.4). The pK_a of HOCl is 7.5, which indicates near equimolar concentrations of both HOCl and hypochlorite anion (OCl^-) at physiological pH. The probe exhibited significant fluorescence quenching (~2.8 fold), accompanied by a fluorescent color change from bright blue to faint blue in the presence of hypochlorite (Figure 5c). The saturation in the emission signal was reached at ~50 μM of hypochlorite addition. On the other hand, we did not observe any significant fluorescence quenching of the probe (without cellulose) upon hypochlorite addition, owing to the spontaneous aggregation of probe molecules in the aqueous medium, which makes the binding site inaccessible to the incoming analyte (Figure 5d). Additionally, in aqueous medium, the probe formed spontaneous agglomerated structures, while the **1. Cell** adduct assembled in a templated ordered arrangement. This change in the morphology/assembly of the probe and **1. Cell** elicited a differential fluorescence response toward hypochlorite.

https://doi.org/10.1021/acsmaterialsau.4c00113
ACS Mater. Au 2025, 5, 308−319

Additionally, the interaction between hypochlorite and probe **1** may yield a structurally distinct product, therefore, the observed fluorescence quenching. This agrees with the well-documented literature, which demonstrates that redox oxidants like HOCl commonly induce oxidative deboronation in arylboronates, leading to the formation of phenolic products. The ultrasensitive naked-eye and fluorometric response of **1. Cell** toward hypochlorite plausibly arises from the amplification effect within the orderly arranged cellulose polymer chain. The **1. Cell** composite utilizes the synergistic effect of multiple number of recognition sites along the cellulose chain to efficiently bind hypochlorite at low concentrations.[40−42] The increased response to NaOCl is attributed to the amplification effect provided by the cellulose polymer chain, which facilitates long-range exciton migration within the templated aggregates. The supramolecularly assembled CTE system in this study is expected to exhibit several distinctive features: Noncovalent interactions facilitate the CTE effect even at low concentrations, enhancing emission efficiency without the need for high molecular density; the incorporation of organic fluorophore induces structural rigidity, promoting effective spatial conjugation and enhancing emission stability; and the self-assembled CTE system demonstrates responsiveness to stimuli (analyte), providing a versatile platform for sensing applications and adaptive luminescent materials.[43] Additionally, cellulose itself remains inert upon the addition of hypochlorite (NaOCl), indicating that the enhanced fluorescence response is specific to the structured interactions within the composite system, with both the probe and cellulose maintaining stability unless in the presence of targeted chemical stimuli. Furthermore, the DLS and FESEM experiments revealed that the hydrodynamic diameter of the composite decreased from 372.17 ± 1.3 nm to 128.25 ± 5.6 nm and the composite dissociated into dispersed small rod-shaped structures in the presence of hypochlorite (Figure S4). This suggests the dissociation of the preformed aggregated composite in the solution, or the distinct product formed might have different self-assembly behavior in the aqueous medium.

Furthermore, the average lifetime of the **1. Cell** in aqueous medium decreased from 5.68 to 4.31 ns upon hypochlorite addition (Figure 6a). Despite the significant reduction in emission intensity, there was only a marginal decrease in the average lifetime of the composite, which continued to exhibit a multiexponential decay pattern upon hypochlorite addition. Furthermore, we also checked the reaction kinetics between the composite and NaOCl via time-dependent fluorescence response in the aqueous medium. The composite could achieve the detection of NaOCl via a decrease in fluorescence intensity (at 440 nm), within a rapid response (1 min), thereby confirming the real-time detection of NaOCl. This could probably be due to the long-chain cellulose biomacromolecule appended with the probe in the **1. Cell** framework, which makes it easier to interact with NaOCl. Structured aggregation of probe molecules along the cellulose backbone enhances clusteroluminescence via rigidification and enables long-range exciton migration, thereby increasing detection sensitivity and yielding a stable, reliable response to hypochlorite.[44]

Additionally, we prepared the composites of the probe with water-soluble cellulose derivatives such as PVA, and HEC and investigated the fluorescence response toward hypochlorite (Figure 6b). We observed that the extent of fluorescence quenching of the composites was negligible when compared to

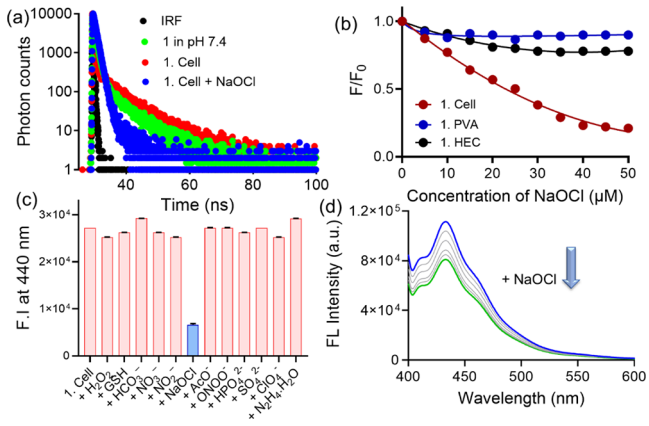

Figure 6. (a) Fluorescence lifetime of probe **1**, **1. Cell** (λ_{ex} = 390 nm) and hypochlorite addition at 440 nm in water. (b) Change in fluorescence intensity of different biopolymer.cellulose composite in the presence of hypochlorite (0−50 μM) in water. (c) Bar plot showing selectivity via the fluorescence intensity of **1. Cell** (at 440 nm) upon addition of relevant analytes (10 equiv) in water. (d) Fluorescence spectra of probe **1** (10 μM, λ_{ex} = 390 nm) upon hypochlorite addition (0−50 μM) in ethanol.

1. Cell composite. Furthermore, we recorded the fluorescence spectra of the **1. Cell** in the presence of a wide range of competitive analytes, such as ROS, HSO_3^-, NO_3^-, NO_2^-, GSH, and so on (Figures 6c and S5). Even at higher concentrations, these analytes did not show any noticeable change in emission intensity, and neither the visible color nor the fluorescence color change. Only hypochlorite could elicit a fluorescent response (quenching) toward the probe. Although boronates can react with H_2O_2, the reaction is slow (rate constant ∼1 $M^{-1}s^{-1}$, while hypochlorite reacts approximately 1,000 times faster, yielding a stable phenolic product with high efficiency.[45,46] Peroxynitrite (ONOO), though reactive, follows a partially radical-based pathway with boronates, leading to lower phenolic product yield (80−85%) and minor radical byproducts.[46] The high selectivity of the probe for ClO likely arises from steric and matrix constraints within the boronate ester-cellulose composite, which limit the ONOO accessibility. These properties ensure rapid, specific ClO detection, even in complex environments with H_2O_2 and ONOO. Meanwhile, there was a good linear relationship between the fluorescence of the probe at 440 nm and the added hypochlorite (50 μM), which indicates that the present system can be employed for the quantitative detection of hypochlorite in aqueous medium. Nevertheless, we also evaluated the fluorescence response of the composite toward hypochlorite across varying pH conditions. We observed that the probe could effectively detect hypochlorite in the pH range 4−10, with a maximum response at pH 7.4. The diminished fluorescence response of the **1. Cell** in highly acidic medium could be attributed to the instability of the formed boronate ester.[47] The above results suggests that although the probe **1** displayed a higher fluorescence response toward NaOCl (OCl-) over HOCl, it could also respond to $HOCl/ClO^-$ with sufficient sensitivity as the pH changed from 4.00 to 10.00. We can therefore conclude that **1. Cell** composite could detect hypochlorite in a range covering the whole physiological pH (biologically relevant pH conditions).

Furthermore, we recorded the fluorescence spectra of probe **1** in the presence of hypochlorite in organic medium, ethanol. We observed negligible quenching of fluorescence intensity

https://doi.org/10.1021/acsmaterialsau.4c00113
ACS Mater. Au 2025, 5, 308−319

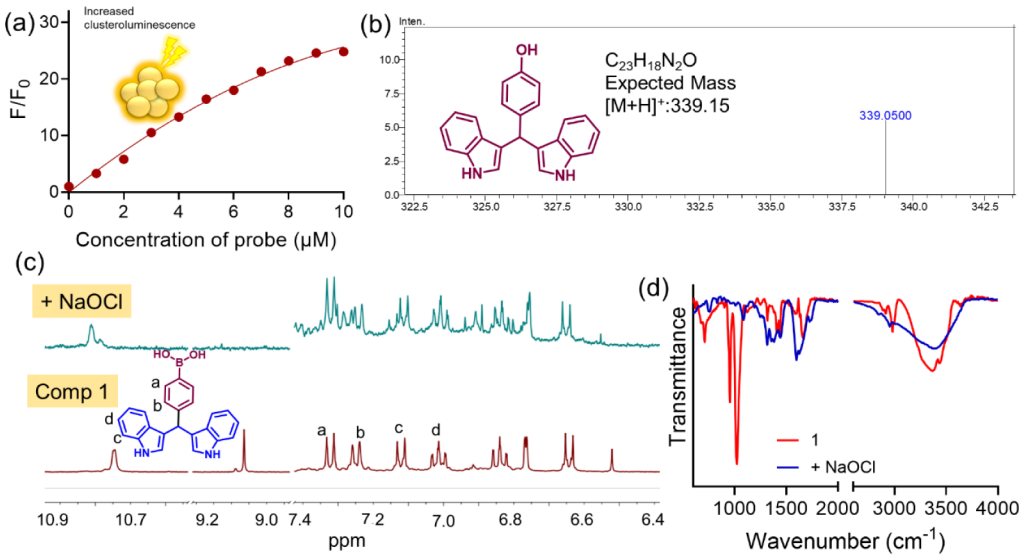

Figure 7. (a) Point plot of change in fluorescence intensity (F/F_o) vs different concentrations of probe **1** in aqueous medium. (b) LC-MS spectra of **1** upon hypochlorite addition. (c) Partial ^{1}H NMR of probe **1** in the presence of hypochlorite in DMSO-d_6. (d) FTIR spectra of probe **1** upon hypochlorite addition.

(∼1.4 fold) at the emission band centered at 434 nm (Figure 6d). This could be due to the reduced solvation and nucleophilicity of ethanol, which hinders the efficient conversion of probe **1** into the corresponding phenolic product. In contrast, water, having high polarity, significantly enhances the solvation of probe **1**, while its strong nucleophilicity facilitates the efficient oxidation of probe **1** to phenolic product, in the presence of hypochlorite. Therefore, we observed a significant fluorescence response in aqueous medium.

Mechanistic Investigation with Hypochlorite

We recorded the fluorescence spectra of the cellulose at different concentrations of the probe (dopant) in an aqueous medium (Figure 7a). It was observed that the fluorescence intensity at 440 nm linearly increased with the increasing concentration of the probe, suggesting that the clusteroluminescence effect of cellulose is promoted by the addition of the probe (as an organic dopant). More concentration of the probe will increase the rigidity of the cellulose backbone, thereby strengthening the clusteroluminescence. The optimized luminescence response was achieved at a probe concentration of 8 μM, beyond which further increase in concentration did not enhance the luminescence.[48,49] Furthermore, we recorded the IR spectra of the probe in the presence of hypochlorite. Thestretching frequencies of the −OH groups of the probe at around 3361 cm^{-1}, shifted to higher frequencies (3410 cm^{-1}) and the characteristic IR bands of the probe was found to be shifted to lower frequencies, thereby suggesting the interaction between the probe and the hypochlorite (Figure 7d). Furthermore, the mass spectra also shows a prominent peak at m/z = 339.05 (Figures 7b and S6), which indicates the conversion of the phenylboronic acid moiety to phenol moiety. To delve into the mode of interaction, we recorded the ^{1}H NMR of the probe **1. Cell** in the presence of hypochlorite (1 equiv) in DMSO-d_6 (Figure 7c). The ^{1}H NMR spectra revealed significant downfield shift of the protons labeled as "a," "b," "c," and "d," which is probably due to the oxidative transformation of the electron-withdrawing C−B bond to the electron-donating C−O bond. Such mechanism has been previously reported by Xu and Duan et al.[5,50] The above observations suggest that the boronic acid functionality of the probe undergoes an oxidative transformation to form phenol.

In addition, we recorded the ^{1}H NMR spectra of the probe in the presence of cellulose in DMSO-d_6: D_2O mixture. The NMR spectra of native cellulose displayed a broad signal at 3.14−3.15 ppm, which can be attributed to the −CH group of cellulose. The cellulose −OH peaks, however, were not visible due to overlap with the water signal,[51] and the cellulose-bound proton resonances are characterized by low intensity.[52] In contrast, the probe alone exhibited broad aromatic peaks, likely caused by aggregation. When cellulose was combined with the probe (**1. Cell**), the cellulose peaks exhibited a downfield shift, and simultaneously, the signals of the probe were also downfield shifted. These observations strongly suggest mutual interaction between the probe and cellulose (Figure S7)

The probe **1** contains two distinct binding sites: a boronic acid moiety and an indole group, which simultaneously interact with cellulose via covalent boronate ester formation and hydrogen bonding, respectively. This dual-site attachment to cellulose induces significant rigidification within the cellulose matrix, enhancing its intrinsic clusteroluminescence. Upon exposure to hypochlorite, the boronate ester linkage undergoes oxidative cleavage, producing phenolic derivatives. This cleavage disrupts the cluster-luminescent architecture of cellulose, thereby leading to observable fluorescence quenching.

Based on the above observations, we presumed a plausible mechanism for hypochlorite sensing (Scheme S2). Upon addition of NaOCl, a chemodosimetric interaction takes place at the boronic ester binding site, which triggers the cleavage of the aryl boronic acid to the phenol functionality. In aryl boronic acids and their esters, the vacant p-orbital (Lewis acid) of boron is susceptible to nucleophilic attack by HOCl/OCl, leading to migration of the aryl group (bisindolyl) from boron to oxygen. This event is followed by oxidative deboronation, which converts the boronic acid into an aryl alcohol and boric acid in the aqueous medium.[53] Such a borono-dakin oxidation

https://doi.org/10.1021/acsmaterialsau.4c00113
ACS Mater. Au 2025, 5, 308−319

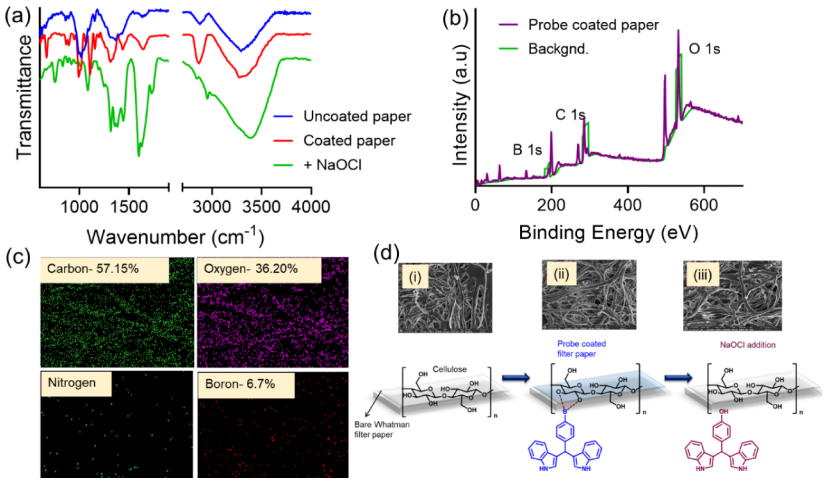

Figure 8. (a) FTIR of cellulose paper, paper grafted probe **1**, and hypochlorite addition. (b) XPS survey spectra of the paper-grafted probe. (c) Schematic representation of a paper-based device for hypochlorite detection and FESEM images of (i) Bare Whatman paper, (ii) paper grafted probe. (iii) Hypochlorite addition to paper grafted probe. (d) EDAX mapping of paper grafted cellulose.

mechanism has been reported earlier for ROS detection by boronic-acid based probes.[54,55]

Application towards Real-Life Samples

Hypochlorite plays a crucial role in disinfection across various sectors, with applications ranging from municipal water treatment at 1−5 mg/L to ensure drinking water safety, to maintaining sanitation in swimming pools at 2−4 mg/L, and reducing microbial contamination on food-processing surfaces at concentrations of 50−200 mg/L.[56,57] However, the improper release of industrial wastes containing hypochlorite (ClO^-) poses a risk of water resource contamination, and its growing use in food and dairy products to inhibit microbial activity further underscores the need for robust methods to monitor ClO^- levels in diverse environmental and food matrices. Developing effective detection methods is therefore essential to safeguarding public health and environmental quality.

Therefore, we explored the practicability of **1. Cell**, by analyzing different real-life water samples such as swimming pools, disinfecting agents, tap water etc. Before the recovery experiments, all the samples were filtered to remove small particulate matter, and recovery studies were obtained by repeating the experiment three times under identical conditions. Further, known concentrations of hypochlorite ranging from 10 to 80 μM were precisely spiked into each sample matrix, including water samples, and disinfectants. Following this, the fluorescence responses of the **1. Cell** composite toward the spiked samples were monitored at 440 nm and an external calibration curve was independently generated for each matrix. The spiked samples showed consistent linear changes in fluorescence intensity. Furthermore, the quantification of hypochlorite in the spiked samples demonstrated good recovery values ranging from 96.2% to 102.56%, with relative standard deviation (RSD) below 5% (Figure S8). These superior recovery values, coupled with minimal RSD values, underscore the analytical robustness and precision of the proposed method, confirming its efficacy for the reliable quantification of trace hypochlorite levels in complex sample matrices.

Chemically Modified Paper Strips for On-Location Analysis

High levels of hypochlorite (ClO^-) in organisms can damage biomolecules, leading to diseases like atherosclerosis, arthritis, and cancer, and yet the lack of a reliable detection method impedes understanding its pathogenic mechanisms. Commonly found in disinfectants and bleach, hypochlorite posts health risks at concentrations from 10^{-5} to 10^{-2} M, making a sensitive detection method vital to mitigate these hazards. Accurate detection aids in environmental studies and water quality assessment and industrial applications, thereby contributing to advancements in health, environmental science, and technology. Therefore, cellulose paper (Whatman filter paper) was chosen as the sensor platform due to its advantageous attributes, including affordability, water compatibility, portability, and disposability.

We activated the Whatman #6 filter paper (see Supporting Information) and functionalized it with probe **1** in pH 7.4 medium. The chemical modifications of the cellulose paper was characterized by FT-IR, EDAX and XPS. The FTIR spectra of pristine paper exhibits characteristic IR bands around 3300 and 2874 ascribed to the O−H and C−H bonds respectively (Figure 8a). The successful grafting of the cellulose paper with probe via the boronate ester linkage was evidenced by the bands positioned at 1428 and 1322 cm^{-1}, which are attributed to B−O stretching and C−B stretching, respectively. Additionally, the XPS survey scan spectra and EDAX mapping images of the probe-coated paper confirms the presence of O, C, and B, N elements (Figure 8b,c). Furthermore, the FESEM images reveal that the integrity of the cellulose fibers was unaffected by the chemical modifications, which implies that the paper was unwrinkled and, hence, could be employed as a sensor device (Figure 8d). The stability of the paper strips was then evaluated before spectroscopic analysis and sensing studies with hypochlorite. No significant detectable change in color intensity of the precoated paper was noticed, even after 6 days (Figure 9a), which indicates that the coated paper was quite stable under ambient conditions (room temperature) and could be employed as a sensor device for the detection of hypochlorite.

Furthermore, these probe-coated paper strips displayed bright blue fluorescence under UV light (>365 nm), which displayed concentration-dependent gradual quenching of blue

https://doi.org/10.1021/acsmaterialsau.4c00113
ACS Mater. Au 2025, 5, 308−319

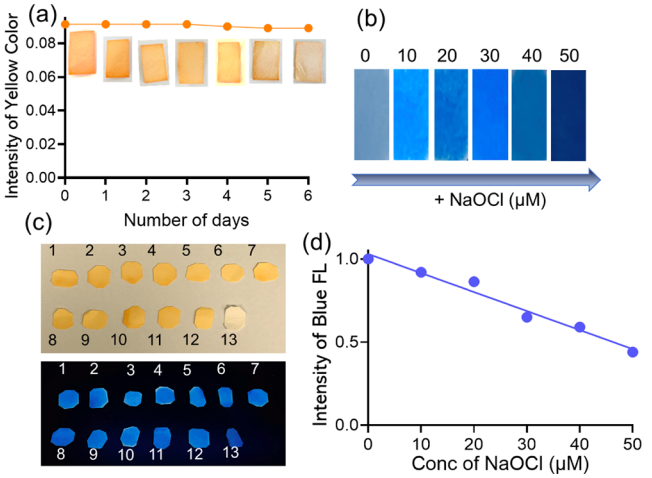

Figure 9. (a) Absorbance of probe coated paper at 495 nm for 6 days. (b) Change in color of paper strips coated with **1** upon addition of hypochlorite ions (the concentration increases from the left to right) under UV light (c) Picture captured under day light and UV light after the addition of hypochlorite onto precoated Whatman paper. (d) Changes in color intensity of precoated paper upon addition of hypochlorite (0−50 μM), quantified by *ImageJ* software.

fluorescence in the presence of hypochlorite (Figure 9b). The changes in intensity could be quantified using image processing software ImageJ (Figure 9d). By employing this sensor device, we investigated the colorimetric and fluorometric detection of relevant biological and ionic analytes (Analytes 1−13, see Supporting Information), and it was observed that only hypochlorite could induce naked-eye color change from pale yellow to colorless, and fluorescent color change from bright blue to faint blue (Figure 9c).

CONCLUSION

This work involves the functionalization of biocompatible polysaccharide, cellulose, by grafting BIM-based boronic acid probe via dynamic boronate ester formation in a aqueous medium. The fluorescence intensity of the probe exhibited significant enhancement (~29.3 fold) in the presence of cellulose, owing to the increased clusteroluminescence of cellulose in the presence of the probe. Furthermore, we employed this composite for colorimetric and fluorescence detection of hypochlorite ions. Mechanistic investigations reveal the oxidative transformation of arylboronates to the corresponding phenol product in the presence of hypochlorite. The differential fluorescence response is attributed to the distinct aggregate formations of the probe **1** and **1. Cell**, where spontaneous aggregation (in case of probe **1**) hampers the interaction, while templated aggregate in the **1. Cell** composite promotes the interaction with hypochlorite in aqueous medium. Fortunately, we developed a paper-based device for the real-time selective detection of hypochlorite and also characterized the activated paper strips through FTIR, SEM, EDAX and XPS. The design methodology outlined in this paper provides a valuable reference for the construction of cellulose-based sensing devices. In addition, the cellulose polymer-based fluorescent chemosensor demonstrates significant advantages over the small molecular sensors, including enhanced sensitivity, substantial signal amplification, superior formability, and the capability to integrate multiple output modalities. This study presents a observation of clusteroluminescence enhancement in solution, a phenomenon traditionally observed only in the solid state. By introducing a boron-containing probe that binds with cellulose, even at lower concentrations to form boronate ester linkages, we achieve significant fluorescence "turn-on" in solution state at room temperature. Our findings reveal that the probe acts as a organic dopant, creating a densely cross-linked network within the cellulose, which mimics the aggregation-induced emission properties of clusteroluminescence under solution conditions. This novel approach expands the potential applications of clusteroluminescent materials, enabling their use in fluid-based systems such as bioimaging, sensing, and diagnostics, where solution-phase fluorescence enhancement is often more practical and preferable. The results thus open up a new pathway for achieving clusteroluminescent effects in solution, marking a significant advancement in the field of fluorescence materials.

ASSOCIATED CONTENT

Supporting Information

The Supporting Information is available free of charge at https://pubs.acs.org/doi/10.1021/acsmaterialsau.4c00113.

Experimental section, Scheme of synthesis and characterization of compounds, Mechanism of NaOCl detection, Normalized excitation spectra of probe **1** (10 μM) in THF (λ_{em} = 435 nm) and water (λ_{em} = 449 nm) medium, DLS and FESEM images of probe **1** (10 μM) in water, Change in fluorescence intensity (F/F_0) of probes **1**, **2**, and **3** with cellulose in aqueous medium, DLS and FESEM images of **1.Cell** upon hypochlorite addition in water, Fluorescence intensity of **1. Cell** (at 440 nm) upon addition of metal ions (10 equiv) in water, Fluorescence intensity of **1. Cell** (at 440 nm) upon addition of relevant anions (10 equiv) in water. HRMS of 1. Cell in the presence of NaOCl, Partial ^{1}H NMR of probe **1**, **1. Cell** and cellulose in the DMSO-d_6: D_2O mixture, change in fluorescence intensity of 1.Cell upon addition of hypochlorite in different real-life water samples, Table displaying quantitative estimation (detection limit (in μM), recovery values and relative standard deviations) of hypochlorite in real-life samples. Comparison table of various hypochlorite sensors reported in the literature (PDF)

AUTHOR INFORMATION

Corresponding Author

Nilanjan Dey − *Department of Chemistry, BITS-Pilani Hyderabad Campus, Hyderabad 500078, India;* orcid.org/0000-0002-3988-1509; Email: nilanjandey.iisc@gmail.com, nilanjan@hyderabad.bits-pilani.ac.in

Author

Rikitha S Fernandes − *Department of Chemistry, BITS-Pilani Hyderabad Campus, Hyderabad 500078, India*

Complete contact information is available at: https://pubs.acs.org/10.1021/acsmaterialsau.4c00113

Notes

The authors declare no competing financial interest.

https://doi.org/10.1021/acsmaterialsau.4c00113
ACS Mater. Au 2025, 5, 308−319

REFERENCES

(1) Jin, K.; Song, G.; Diao, H.; Zhang, X.; Ji, X.; Zhang, J.; Zhang, J. Hydrogen-Bond Assisted Nonconventional Photoluminescence of Crystalline and Amorphous Cellulose. *Cellulose* **2023**, *30* (13), 8139−8150.

(2) Zhao, Z.; Chen, X.; Wang, Q.; Yang, T.; Zhang, Y.; Yuan, W. Z. Sulphur-Containing Nonaromatic Polymers: Clustering-Triggered Emission and Luminescence Regulation by Oxidation. *Polym. Chem.* **2019**, *10* (26), 3639−3646.

(3) Li, Q.; Wang, X.; Huang, Q.; Li, Z.; Tang, B. Z.; Mao, S. Molecular-Level Enhanced Clusterization-Triggered Emission of Nonconventional Luminophores in Dilute Aqueous Solution. *Nat. Commun.* **2023**, *14* (1), 409.

(4) Zhang, H.; Zhao, Z.; McGonigal, P. R.; Ye, R.; Liu, S.; Lam, J. W. Y.; Kwok, R. T. K.; Tang, B. Z.; Xie, J.; Rogach, A. L.; Tang, B. Z. Clusterization-Triggered Emission: Uncommon Luminescence from Common Materials. *Mater. Today* **2020**, *32*, 275−292.

(5) Xu, Q.; Lee, K. A.; Lee, S.; Lee, K. M.; Lee, W. J.; Yoon, J. A Highly Specific Fluorescent Probe for Hypochlorous Acid and Its Application in Imaging Microbe-Induced HOCl Production. *J. Am. Chem. Soc.* **2013**, *135* (26), 9944−9949.

(6) Marco-Dufort, B.; Iten, R.; Tibbitt, M. W. Linking Molecular Behavior to Macroscopic Properties in Ideal Dynamic Covalent Networks. *J. Am. Chem. Soc.* **2020**, *142* (36), 15371−15385.

(7) Huang, S.; Kong, X.; Xiong, Y.; Zhang, X.; Chen, H.; Jiang, W.; Niu, Y.; Xu, W.; Ren, C. An Overview of Dynamic Covalent Bonds in Polymer Material and Their Applications. *Eur. Polym. J.* **2020**, *141*, 110094.

(8) Jin, S.; Cao, J.; Li, J.; Han, J.; Mei, C.; Li, K.; Xiao, H. Biomass-Based Functional Film Integrated with Nitrogen-Coordinating Boronic Ester and Cellulose-Barium Titanate Nanohybrids. *Ind. Crops Prod.* **2022**, *189*, 115765.

(9) Borsley, S.; Poss, G.; Spicer, R. L.; Boudin, E.; Kay, E. R. Switchable Selectivity within a Series of Boronate Esters for Dynamic Covalent Exchange in Nonaqueous Solvents. *Supramol. Chem.* **2018**, *30* (9), 772−781.

(10) Yang, C.; Feng, W.; Li, Y.; Tian, X.; Zhou, Z.; Lu, L.; Nie, Y. Graphene Oxide Based Ratiometric Fluorescent Paper Sensor for Hypochlorous Acid Visual Detection. *J. Photochem. Photobiol. A Chem.* **2019**, *375*, 141−147.

(11) Fernandes, R. S.; Kumari, J.; Gangopadhyay, A.; Sriram, D.; Dey, N. Tailoring Bisindolyl Methane Derivatives for Dual Applications: Substituent-Directed Probing of Cyanide Ions and Anti-Tubercular Activity. *J. Mol. Liq.* **2024**, *410*, 125266.

(12) Fernandes, R. S.; Dey, N. Oxidized Bis (Indolyl) Methane Derivatives with Diverse Signaling Units: An Excitation-Dependent Fluorescence Response toward Heavy Metal Pollutants in an Aqueous Medium. *Ind. Eng. Chem. Res.* **2023**, *62* (50), 21536−21545.

(13) Wang, R.; Bian, Z.; Zhan, D.; Wu, Z.; Yao, Q.; Zhang, G. Boronic Acid-Based Sensors for Small-Molecule Reactive Species: A Review. *Dyes Pigm.* **2021**, *185*, 108885.

(14) Fernandes, R. S.; Dey, N. Metal Ion Responsive Bifunctional Bis (Indolyl) Methane Derivative: Excitation-Triggered Alteration in the Sensing Behavior. *Mater. Chem. Phys.* **2023**, *302*, 127637.

(15) Fernandes, R. S.; Dey, N. Single-Benzene-Based Fluorophores (SBBFs) with Green Luminescence: Improved Sensitivity Towards Cysteine Both in Solution and Solid State. *Mater. Today Chem.* **2024**, *36*, 101850.

(16) Fernandes, R. S.; Dey, N. Exploring the Synergistic Effect of Aggregation and Hydrogen Bonding: Fluorescent Probe for Dual Sensing of Phytic Acid and Uric Acid. *J. Mater. Chem. B* **2024**, *12*, 11789−11799.

(17) Hirose, T.; Higashiguchi, K.; Matsuda, K. Self-Assembly and Aggregate-Induced Enhanced Emission of Amphiphilic Fluorescence Dyes in Water and in the Solid State. *Chem.−asian J.* **2011**, *6* (4), 1057−1063.

(18) Sun, X.; Chapin, B. M.; Metola, P.; Collins, B.; Wang, B.; James, T. D.; Anslyn, E. V. The Mechanisms of Boronate Ester Formation and Fluorescent Turn-On in Ortho-Aminomethylphenylboronic Acids. *Nat. Chem.* **2019**, *11* (9), 768−778.

(19) Ogunsipe, A.; Chen, J. Y.; Nyokong, T. Photophysical and Photochemical Studies of Zinc (II) Phthalocyanine Derivatives—Effects of Substituents and Solvents. *New J. Chem.* **2004**, *28* (7), 822−827.

(20) Bangar, S. P.; Harussani, M. M.; Ilyas, R. A.; Ashogbon, A. O.; Singh, A.; Trif, M.; Jafari, S. M. Surface Modifications of Cellulose Nanocrystals: Processes, Properties, and Applications. *Food Hydrocoll.* **2022**, *130*, 107689.

(21) Hu, H.; Wang, F.; Yu, L.; Sugimura, K.; Zhou, J.; Nishio, Y. Synthesis of Novel Fluorescent Cellulose Derivatives and Their Applications in Detection of Nitroaromatic Compounds. *ACS Sustainable Chem. Eng.* **2018**, *6* (1), 1436−1445.

(22) Brooks, W. L.; Sumerlin, B. S. Synthesis and Applications of Boronic Acid-Containing Polymers: From Materials to Medicine. *Chem. Rev.* **2016**, *116* (3), 1375−1397.

(23) Fernandes, R. S.; Dey, N. Polarity-Independent Temperature-Induced Reversible Fluorescence Switching of Organic Nanoparticles: Application to Intracellular Temperature Imaging. *ACS Appl. Nano Mater* **2023**, *6* (7), 5168−5176.

(24) Araki, J. Electrostatic or Steric?−Preparations and Characterizations of Well-Dispersed Systems Containing Rod-Like Nanowhiskers of Crystalline Polysaccharides. *Soft Matter* **2013**, *9* (16), 4125−4141.

(25) Ye, X.; Wang, H.; Yu, L.; Zhou, J. Aggregation-Induced Emission (AIE)-Labeled Cellulose Nanocrystals for the Detection of Nitrophenolic Explosives in Aqueous Solutions. *Nanomaterials* **2019**, *9* (5), 707.

(26) Fernandes, R. S.; Kumari, J.; Sriram, D.; Dey, N. Fluorescent Nanoassembly of Tetrazole-Based Dyes with Amphoteric Surfactants: Investigation of Cyanide Sensing and Antitubercular Activity. *ACS Appl. Bio Mater,* **2023**, *6* (10), 4158−4167.

(27) Vu, H.; Woodcock, J. W.; Krishnamurthy, A.; Obrzut, J.; Gilman, J. W.; Coughlin, E. B. Visualization of Polymer Dynamics in Cellulose Nanocrystal Matrices Using Fluorescence Lifetime Measurements. *ACS Appl. Mater. Interfaces* **2022**, *14* (8), 10793−10804.

(28) DiCesare, N.; Lakowicz, J. R. Fluorescent Probe for Monosaccharides Based on a Functionalized Boron-Dipyrromethene with a Boronic Acid Group. *Tetrahedron Lett.* **2001**, *42* (52), 9105−9108.

(29) DiCesare, N.; Adhikari, D. P.; Heynekamp, J. J.; Heagy, M. D.; Lakowicz, J. R. Spectroscopic and Photophysical Characterization of Fluorescent Chemosensors for Monosaccharides Based on N-Phenylboronic Acid Derivatives of 1,8-Naphthalimide. *J. Fluoresc.* **2002**, *12*, 147−154.

(30) Wen, H.; Morris, K. R.; Park, K. Synergic Effects of Polymeric Additives on Dissolution and Crystallization of Acetaminophen. *Pharm. Res.* **2008**, *25*, 349−358.

(31) Zhao, J.; Li, J.; Zeng, Q.; Wang, H.; Yu, J.; Ren, K.; Dai, Z.; Zhang, H.; Zheng, J.; Hu, R. A Chewing Gum Residue-Based Gel with Superior Mechanical Properties and Self-Healability for Flexible Wearable Sensor. *Macromol. Rapid Commun.* **2022**, *43* (13), 2200234.

(32) Smith, M. K.; Northrop, B. H. Vibrational Properties of Boroxine Anhydride and Boronate Ester Materials: Model Systems for the Diagnostic Characterization of Covalent Organic Frameworks. *Chem. Mater.* **2014**, *26* (12), 3781−3795.

(33) Faniran, J. A.; Shurvell, H. F. Infrared Spectra of Phenylboronic Acid (Normal and Deuterated) and Diphenyl Phenylboronate. *Can. J. Chem.* **1968**, *46* (12), 2089−2095.

(34) Das, R. K.; Mohapatra, S. Heteroatom-Doped Carbon Quantum Dots for Ultrasensitive Sensing of Glucosamine and Targeted Imaging of Liver Cancer Cells. *J. Mater. Chem. B* **2017**, *5* (11), 2190−2197.

(35) Cai, C.; Wei, Z.; Huang, Y.; Wang, P.; Song, J.; Deng, L.; Fu, Y. Rigid-Stretchable" Unity of Shape Memory Composites with Fluorescence via Crystallinity Tailoring for Anti-Counterfeiting Application. *Compos. Sci. Technol.* **2021**, *201*, 108524.

https://doi.org/10.1021/acsmaterialsau.4c00113
ACS Mater. Au 2025, 5, 308−319

(36) Crawshaw, J.; Bras, W.; Mant, G. R.; Cameron, R. E. Simultaneous SAXS and WAXS Investigations of Changes in Native Cellulose Fiber Microstructure on Swelling in Aqueous Sodium Hydroxide. *J. Appl. Polym. Sci.* **2002**, *83* (6), 1209−1218.
(37) Liu, Q.; Chen, C.; Du, M.; Wu, Y.; Ren, C.; Ding, K.; Song, M.; Huang, C. Porous Hexagonal Boron Nitride Sheets: Effect of Hydroxyl and Secondary Amino Groups on Photocatalytic Hydrogen Evolution. *ACS Appl. Nano Mater.* **2018**, *1* (9), 4566−4575.
(38) Matsoso, B. J.; Ranganathan, K.; Mutuma, B. K.; Lerotholi, T.; Jones, G.; Coville, N. J. Synthesis and Characterization of Boron Carbon Oxynitride Films with Tunable Composition Using Methane, Boric Acid, and Ammonia. *New J. Chem.* **2017**, *41* (17), 9497−9504.
(39) Zhang, Y.; Zeng, X.; Wu, H.; Li, Z.; Ren, T.; Zhao, Y. The Tribological Chemistry of a Novel Borate Ester Additive and Its Interaction with ZDDP Using XANES and XPS. *Tribol. Lett.* **2014**, *53*, 533−542.
(40) Sun, H.; Xu, Q.; Xu, C.; Zhang, Y.; Ai, J.; Ren, M.; Wang, S.; Kong, F. A highly sensitive and low toxicity cellulose-based fluorescent polymer for H_2S detection in cells, zebrafish and food samples. *Anal. Methods* **2023**, *15* (26), 3156−3160.
(41) Wu, C.; Zheng, Y.; Szymanski, C.; McNeill, J. Energy Transfer in a Nanoscale Multichromophoric System: Fluorescent Dye-Doped Conjugated Polymer Nanoparticles. *J. Phys. Chem. C* **2008**, *112* (6), 1772−1781.
(42) Nawaz, H.; Tian, W.; Zhang, J.; Jia, R.; Chen, Z.; Zhang, J. Cellulose-Based Sensor Containing Phenanthroline for the Highly Selective and Rapid Detection of Fe^{2+} Ions with Naked Eye and Fluorescent Dual Modes. *ACS Appl. Mater. Interfaces* **2018**, *10* (2), 2114−2121.
(43) Zhang, M.; Cheng, Y.; Zhang, T.; Liang, B.; Wei, X.; Wang, P.; Xia, D.; Yan, X. A Clusteroluminescent Supramolecular Polymer Network Constructed by Pillararene and Its Application in Information Encryption. *Aggregate* **2024**, *5* (5), No. e608.
(44) Singh, A.; Dhau, J. S.; Kumar, R.; Badru, R.; Kaushik, A. Exploring Fluorescence Properties of Tellurium-Containing Molecules and Their Advanced Applications. *Phys. Chem. Chem. Phys.* **2024**, *26*, 9816−9847.
(45) Kalyanaraman, B.; Hardy, M.; Zielonka, J. A Critical Review of Methodologies to Detect Reactive Oxygen and Nitrogen Species Stimulated by NADPH Oxidase Enzymes: Implications in Pesticide Toxicity. *Curr. Pharmacol. Rep.* **2016**, *2*, 193−201.
(46) Zielonka, J.; Sikora, A.; Hardy, M.; Joseph, J.; Dranka, B. P.; Kalyanaraman, B. Boronate Probes as Diagnostic Tools for Real-Time Monitoring of Peroxynitrite and Hydroperoxides. *Chem. Res. Toxicol.* **2012**, *25* (9), 1793−1799.
(47) Phyo, P.; Gu, Y.; Hong, M. Impact of Acidic pH on Plant Cell Wall Polysaccharide Structure and Dynamics: Insights into the Mechanism of Acid Growth in Plants from Solid-State NMR. *Cellulose* **2019**, *26*, 291−304.
(48) Chu, B.; Zhang, H.; Hu, L.; Liu, B.; Zhang, C.; Zhang, X.; Tang, B. Z. Altering Chain Flexibility of Aliphatic Polyesters for Yellow-Green Clusteroluminescence in 38 % Quantum Yield. *Angew. Chem.* **2022**, *134* (6), No. e202114117.
(49) Zhang, Z.; Xiong, Z.; Chu, B.; Zhang, Z.; Xie, Y.; Wang, L.; Sun, J. Z.; Zhang, H.; Zhang, X.-H.; Tang, B. Z. Manipulation of Clusteroluminescence in Carbonyl-Based Aliphatic Polymers. *Aggregate* **2022**, *3* (6), No. e278.
(50) Duan, Y. M.; Wang, S.; Cao, F.; Zhang, Q.; Chen, S.; Zhang, Y. B.; Wang, K. P.; Hu, Z. Q. Facile and Highly Selective Ratiometric Fluorescence Probe Based on Benzo [5] Helicene for the Detection of Hypochlorous Acid. *Ind. Eng. Chem. Res.* **2020**, *59* (2), 992−999.
(51) Kuroda, K.; Kunimura, H.; Fukaya, Y.; Ohno, H. ^{1}H NMR Analysis of Cellulose Dissolved in Non-Deuterated Ionic Liquids. *Cellulose* **2014**, *21*, 2199−2206.
(52) Dryś, M.; Koso, T. V.; Kilpeläinen, P. O.; Rinne-Garmston, K. T.; Todorov, A. R.; Wiedmer, S. K.; King, A. W.; King, A. W. T. Structural Characterization of 6-Halo-6-Deoxycelluloses by Direct-Dissolution Solution-State NMR Spectroscopy. *Macromol. Rapid Commun.* **2024**, *45* (13), 2300698.
(53) Kuivila, H. G.; Benjamin, L. E.; Murphy, C. J.; Price, A. D.; Polevy, J. H. Electrophilic Displacement Reactions. XIV. Two Novel Reactions Involving Areneboronic Acids and Halogens. *J. Org. Chem.* **1962**, *27* (3), 825−829.
(54) Graham, B. J.; Windsor, I. W.; Gold, B.; Raines, R. T. Boronic Acid with High Oxidative Stability and Utility in Biological Contexts. *Proc. Natl. Acad. Sci. U. S. A.* **2021**, *118* (10), No. e2013691118.
(55) Pak, Y. L.; Park, S. J.; Wu, D.; Cheon, B.; Kim, H. M.; Bouffard, J.; Yoon, J. N-Heterocyclic Carbene Boranes as Reactive Oxygen Species-Responsive Materials: Application to the Two-Photon Imaging of Hypochlorous Acid in Living Cells and Tissues. *Angew. Chem.* **2018**, *130* (6), 1583−1587.
(56) Honarbakhsh, A.; Azma, A.; Nikseresht, F.; Mousazadeh, M.; Eftekhari, M.; Ostovari, Y. Hydro-Chemical Assessment and GIS-Mapping of Groundwater Quality Parameters in Semi-Arid Regions. *J. Water Supply Res. Technol.* **2019**, *68* (7), 509−522.
(57) Pereira, S. S. P.; Oliveira, H. M. D.; Turrini, R. N. T.; Lacerda, R. A. Disinfection with Sodium Hypochlorite in Hospital Environmental Surfaces in the Reduction of Contamination and Infection Prevention: A Systematic Review. *Rev. Esc. Enferm.* **2015**, *49*, 0681−0688.

https://doi.org/10.1021/acsmaterialsau.4c00113
ACS Mater. Au 2025, 5, 308−319